HHS Public Access

Author manuscript

J Colloid Interface Sci. Author manuscript; available in PMC 2016 December 01.

Published in final edited form as:

J Colloid Interface Sci. 2015 December 1; 459: 264–272. doi:10.1016/j.jcis.2015.07.073.

Insights into the Synthesis of Layered Double Hydroxide (LDH) Nanoparticles: Part 1. Optimization and Controlled Synthesis of Chloride-Intercalated LDH

Xiaodi Sun[a], **Erica Neuperger**[a], and **Sandwip K. Dey**[a,b,*]

[a]School for Engineering of Matter, Transport and Energy, Center for Interventional Biomaterials, Ira Fulton College of Engineering, Arizona State University, Tempe, AZ 85281, USA

[b]School of Electrical, Computer and Energy Engineering, Ira Fulton College of Engineering, Arizona State University, Tempe, AZ 85281, USA

Abstract

Layered double hydroxide (LDH) nanoparticles have excellent anion-intercalating property, and their potential as theranostic nanovectors is high. However, understanding of the control of the mean particle size (MPS) and achievement of monodispersed particle size distribution (PSD) remains elusive. Herein, with the aid of statistical design of experiments on a model system of Cl^--intercalated (Zn, Al)-LDH, controlled synthesis of single crystalline nanoparticles using the coprecipitation method followed by hydrothermal treatment (HT) is achieved in three steps. First, a 2^{4-1} design enabled the identification of influential parameters for MPS (i.e., salt concentration, molar ratio of carbonate to aluminum, solution addition rate, and interaction between salt concentration and stirring rate) and PSD (i.e., salt concentration and stirring rate), as well as the optimum coprecipitation conditions that result in a monodispersed PSD (i.e., low salt concentration and high stirring rate). Second, a preliminary explanation of the HT was suggested and the optimum HT conditions for obtaining ideal Gaussian PSD with chi-squared (χ^2) < 3 were found to be 85 °C for 5 h. Third, using a central composite design, a quantitative MPS model, expressed in terms of the significant factors, was developed and experimentally verified to synthesize nearly monodispersed LDH nanoparticles with MPS ~200–500 nm.

Graphical Abstract

*Corresponding Author: sandwip.dey@asu.edu.

Note

The authors declare no competing financial interest.

ASSOCIATED CONTENT

Supporting Information

Supporting information available: Experimental design and results of (1) Unreplicated resolution IV 2^{4-1} fractional factorial screening design, and (2) Central composite design to develop a quantitative response surface of MPS.

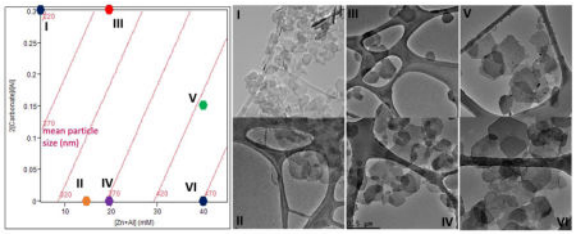

With the aid of design of experiments, a mean particle size (MPS) model, expressed in the significant factors, was developed and experimentally verified to synthesize nearly monodispersed Cl^--intercalated (Zn, Al)-LDH nanoparticles with MPS ~ 200–500 nm.

1. INTRODUCTION

Hydrotalcite-like layered double hydroxide (LDH) materials are well-known for their anion-intercalating properties, and the general empirical formula can be denoted as $[M^{2+}_nM^{3+}(OH)_{2+2n}]^+(A^{a-})_{1/a}{\cdot}xH_2O$ (with n = 1-5), where M^{2+} and M^{3+} are divalent and trivalent cations (e.g. $M^{2+} = Mg^{2+}$, Co^{2+}, Zn^{2+}; $M^{3+} = Al^{3+}$, Ga^{3+}, Fe^{3+}, Mn^{3+}, Gd^{3+}, etc.), and A^{a-} is an anion with a negative charge of a. Here, the M^{2+} is octahedrally coordinated by OH^-, with the octahedra sharing edges to form the M^{2+} hydroxide layer. The isomorphous substitution of M^{2+} by M^{3+} renders the layer with positive charges, which are then neutralized by exchangeable anions intercalated between the successive double hydroxide layers, together with water held in the interlayer gallery via hydrogen bonding to the hydroxyls.[1] Their applications in bulk form have been in the areas of catalysis, catalyst support, environmental remediation, and ceramic precursor.[2–7] Recently, LDH nanoparticles (NPs) with different intercalated compounds have exhibited versatility and promises in biomedicine as theranostic nanovector, i.e., particulate nanocarriers having therapeutic and imaging attributes.[8–14] For example, several *in vivo* multimodal imaging studies[15, 16] and a number of *in vivo* studies, using animal models to determine the pharmacokinetics, toxicity, transfection efficiency, and therapeutic efficacy of LDH, have been reported.[17–19]

Among many synthesis methods for LDH, the most versatile is the coprecipitation method.[20] Typically, it consists of precipitating two suitable metal cations in the presence of the intercalating anions and a base. According to the pH variation curve during the coprecipitation process, a couple of useful routes include coprecipitation at varying pH and at constant pH.[21–23] The latter is the most widely used method for LDH preparation due to its main advantage of the minimal formation of undesired metal hydroxides.[20] The coprecipitation is comprised of three steps, (i) mixing of the cations with the base, (ii) homogeneous nucleation due to supersaturation, (iii) seed-assisted growth of LDH on the nucleus.[24] However, from macroscopic point of view, it is impossible to distinguish these individual steps due to significant overlap, especially under supersaturation condition with convection. As a consequence, LDH particles of very different particle sizes and size distributions result. Also, the synthesis window, agglomeration tendency, and stability for each system is different.[25] To date, the only system that has been extensively studied in crystalline NP and monodispersed form has been (Mg, Al)-LDH,[26–30] whereas studies on

other biocompatible systems with physiological relevance[23] (e.g. (Zn, Al)-LDH, (Zn, Fe)-LDH, etc.) are rare despite the fact that Zn-based LDH compositions exhibit higher stability than Mg-based ones.[21] Moreover, conditions that form stable (Mg, Al)-LDH colloidal suspensions can lead to (Zn, Al)-LDH NPs with much enlarged sizes.[31] One study, using a vortex reactor under steady-state conditions and without post-hydrothermal treatment (HT), demonstrated the synthesis of semicrystalline $Zn_2Al(OH)_6(CO_3)_{0.5}{\cdot}2H_2O$ NPs.[32] However, due to the low crystallinity and the presence of strongly-bound carbonate (CO_3^{2-}), the post-synthesis intercalation of relevant anions could become difficult. In general, documented literature does not reflect systematic studies on the effects of synthesis parameters for LDH NPs. Therefore, from both the colloid science point of view and to address the long-term question of whether crystalline LDH systems will be accepted in biomedicine, optimization and control of the synthesis process (i.e., the central theme of this Part 1 paper) and understanding the underlying mechanisms of structure evolution (i.e., the central theme of the following Part 2 paper)[ref] are of primary importance for the reproducible synthesis of biocompatible NPs with controlled mean particle size (MPS) and particle size distribution (PSD).

From the viewpoints of biocompatibility and anion exchangeability, the authors believe that chloride (Cl^-)-intercalated (Zn, Al)-LDH system is an ideal model system; points in favor of this system are:

- **i.** Critical parameters for the synthesis of (Zn, Al)-based LDH NP has not been documented.
- **ii.** To date, several works on the synthesis of (Mg, Al)-LDH NPs have reported the successful control of particle size and achieve crystallinity via post-synthesis HT.[28, 29] This approach may not necessarily apply to other systems (e.g., (Zn, Al)-LDH, (Zn, Fe)-LDH, and (Mg, Fe)-LDH) since crystalline perfection can lead to increased size via Ostwald ripening.[33] Also, a relatively high hydrothermal temperature (T_{HT} > 90 °C) can activate condensation reactions of Zn-OH via dehydration to form additional ZnO phase in aqueous media.[34] Therefore, control of the coprecipitation conditions is also pivotal towards the formation of phase-pure (Zn, Al)-LDH NPs with controlled MPS and PSD.
- **iii.** Due to the strong interaction between the intercalated CO_3^{2-} and the hydroxide matrix layers, CO_3^{2-} facilitates the formation of crystalline LDH.[26, 29, 31] However, as a consequence, it is very difficult to completely replace the CO_3^{2-} with other relevant anions. Thus, the initial synthesis Cl^--intercalated (Zn, Al)-LDH NPs without CO_3^{2-} or only a small amount can facilitate the intercalation of biomedically-relevant molecules via ion exchange.

Herein, for the first time using statistical design of experiments, a robust and reproducible coprecipitation process at constant pH followed by low-temperature HT is reported for the synthesis of stable and crystalline Cl^--intercalated (Zn, Al)-LDH NPs with controlled MPS and narrow PSD; the content of CO_3^{2-} was kept between 0 and 0.3 of the total molar anion-intercalating capacity. First, the critical synthesis parameters for MPS and PSD and their trends were separately identified using a fractional factorial screening design and ideal coprecipitation conditions were determined, followed by the optimization of the HT

conditions. Eventually, using a central composite design, a quantitative MPS model, expressed in terms of the significant factors (salt concentration, molar ratio of carbonate to aluminum, and solution addition rate), was developed and experimentally verified. Another important factor for the synthesis of stable Cl^--intercalated (Zn, Al)-LDH NPs, i.e., the appropriate range of Zn to Al molar ratio, was also studied.

2. MATERIALS AND METHODS

2.1. Materials

Zinc chloride ($ZnCl_2$), aluminum chloride hexahydrate ($AlCl_3{\cdot}6H_2O$), sodium carbonate (Na_2CO_3) and sodium hydroxide (NaOH) were purchased from Sigma (St. Louis, MO, USA), used as received, and stored under nitrogen gas (N_2) environment. Deionized nanopure water (Barnstead, 18.2 MΩ·cm), degassed by boiling, was used for the preparation of all solutions.

2.2. Synthesis and optimization methodology

The coprecipitation at constant pH method was chosen for the synthesis of (Zn, Al)-LDH NPs. In order to prevent the contamination of CO_3^{2-}, all chemicals were stored in a N_2-filled glove box (MBraun Labmaster 130). Also, since the effect of the concentration of CO_3^{2-} on MPS and PSD is one of the parameter of study, all solution preparations and coprecipitations were carried out at room temperature (RT = 25 °C) within the glove box, and the products were withdrawn in sealed hydrothermal bottles. Typically, a 10 ml salt solution of $ZnCl_2$ and $AlCl_3{\cdot}6H_2O$ with a specific molar ratio of Zn to Al of 2:1 and a given total salt concentration, [Zn+Al], and another 10 ml base solution of NaOH containing a specific amount of Na_2CO_3, with the concentration of the NaOH being twice the concentration of [Zn+Al], were simultaneously added into a round-bottom flask (Chemglass 100 ml round bottom flask) at identical rates using burettes, while stirring at a given speed (Magnetic stirrer: manufactured by Barnant Corp., Barrington, IL, Model 700·0111). The stirring rate was calibrated using a strobe tachometer (Strobette Ameter Model 1000). After completion of the addition of 20 ml precursors, stirring continued for another 3 minutes to ensure thorough mixing. Based on the extremely low values of K_{sp} for the hydroxides (at 25 °C, $K_{sp}(Zn(OH)_2) = 4.1\times10^{-17}$ and $K_{sp}(Al(OH)_3) = 1.9\times10^{-33}$), only stoichiometric amounts of NaOH, which gives twice the OH^- with respect to the total salt concentration, were used to avoid: (1) formation of undesired metal hydroxides due to excess of OH^-, (2) unnecessary agglomeration caused by excess of OH^-, and (3) secondary phase of OH^--intercalated LDH. Therefore, the constant-pH coprecipitation condition was achieved by maintaining this fixed ratio of NaOH to the total cation concentration during precipitation; the post-coprecipitation pH measured at ~5.98. The mixture was then transferred into a hydrothermal bottle (PYREX screw cap 100 ml storage bottle), and the HT was carried out at a specific temperature (T_{HT}), for a given period of time (t_{HT}). Finally, the colloidal suspension was cooled to RT, and centrifuged (Eppendorf 5810R) to collect the gel-like Cl^--intercalated (Zn, Al)-LDH NPs.

The optimization of the synthesis parameters and control of synthesis were accomplished in three consecutive steps. The objective of the first step was to ascertain the significant factors

that can influence the LDH NPs' MPS and PSD, and to determine the optimum coprecipitation condition for obtaining monodispersed PSD. The use of CO_3^{2-} as the intercalated anion for the synthesis of (Mg, Al)-LDH NPs has been widely reported. Typically, salt concentration is also a critical parameter in the synthesis of colloidal systems. Other important parameters that need study include the stirring rate and addition rate. The aforementioned screening parameters are easy to control but their effects on MPS and PSD have not been systematically studied. Therefore, in an unreplicated resolution IV 2^{4-1} fractional factorial screening design, the [Zn+Al], 2[CO_3^{2-}]/[Al], stirring rate, and addition rate were the screening parameters with MPS and PSD as the responses. A total of eight runs were generated using JMP Pro. 10.0.0,[35] and conducted randomly following the synthesis procedure described previously. The T_{HT} and t_{HT} for all the screening runs were 70 °C and 7 h, respectively. Here, a relatively low T_{HT} and short t_{HT} were chosen to improve the crystallinity and minimize the alternation of MPS and PSD by coarsening. The experimental design and results are listed in Table 1. The data analysis was performed using JMP Pro. 10.0.0, and the main effects and interaction effects on the MPS and PSD were identified, separately. The optimum coprecipitation conditions that give monodispersed PSD were then determined.

The second step was the optimization of the HT conditions. For a given sample, six hydrothermal experiments, combining two different T_{HT} (70, 85 °C) with three different t_{HT} (3, 5, and 8 h), were completed to find out the optimum HT conditions that provide monodispersed LDH NPs.

In the third step, the synthesis conditions, i.e., the range for [Zn+Al], 2[CO_3^{2-}]/[Al] ratio, stirring rate, and addition rate, were adjusted and shifted towards the region of interest. A face-centered central composite design with two central points (Table S3) was employed to develop a quantitative response surface in which MPS can be controlled through significant factors, i.e., [Zn+Al], 2[CO_3^{2-}]/[Al] ratio, and addition rate. Note, all the experiments were carried out using the optimum coprecipitation and HT conditions. Once the response surface was generated, the validity of the model was tested experimentally.

Additionally, for the synthesis of stable Cl^--intercalated (Zn, Al)-LDH NPs, the appropriate range of Zn to Al molar ratio was studied; input salt solutions with Zn to Al molar ratios of 1:1, 2:1, 3:1 and 4:1 were used.

2.3. Characterization

The colloidal suspension was cooled to RT, centrifuged (Eppendorf 5810R) to collect the gel-like Cl^--intercalated (Zn, Al)-LDH NPs for physicochemical characterization. The crystalline phase information of LDH NPs was obtained by powder X-ray diffraction (XRD; Rigaku D/Max-IIB instrument with Cu-K_α radiation, λ=0.154059 nm) in 2θ range of 7–70°. The elemental compositions of the LDH NPs were then determined by inductively coupled plasma atomic emission spectroscopy (ICP, iCAP 6300 ICP Spectrometer). Dynamic light scattering (DLS, PSS-NICOMP 380 with zeta potential capability) was used to evaluate the particle size and size distribution. The morphology and particle size of LDH NPs were further examined by bright-field transmission electron microscopy (FEG TEM; Philips CM200 with an electron acceleration voltage of 200 kV) to corroborate the DLS results, and

the crystallographic information was obtained by selected area diffraction. To understand the inter-relationship between the surface charges of (Zn, Al)-LDH NPs with different Zn to Al molar ratio, zeta-potential measurements on the LDH NPs were employed.

3. RESULTS AND DISCUSSIONS

3.1. Initial screening of the critical synthesis parameters

In order to determine the significant main effects and interaction effects on MPS and PSD, a total of eight experiments were designed using unreplicated 2^{4-1} fractional factorial screening design (resolution IV) and carried out in a random fashion. To minimize the risk of having an error-dominated fit to the model, and to ensure the reliability of the estimates of the effect in an unreplicated design, the range between the low and high levels of the screening parameters (i.e., [Zn+Al], 2[CO_3^{2-}]/[Al], stirring rate, and addition rate) were chosen to be as large as possible but experimentally practical. Following the coprecipitation and hydrothermal procedures described in the experimental section, Table 1 summarizes the coprecipitation conditions (i.e., range for individual screening factor) of the initial screening experiments along with the results.

Since there is no internal estimate of error (pure error) in an unreplicated design, the sparsity of effects principle is followed, assuming that certain higher order interactions are negligible, and their mean squares are combined to estimate the mean square error. To avoid accidentally pooling the significant higher order interactions for the estimation of the mean square error, a preliminary assessment of the importance of the effects was first carried out by visually inspecting the normal probability plot (Figure S1). The most pronounced significant effects on the influence of MPS are probably [Zn+Al] and 2[CO_3^{2-}]/[Zn+Al] with the absence of any significant higher order interactions.

To complement the result, the significance of the estimates of each main effects and interactions was further judged using a *t*-test for the hypothesis that it equals zero. By setting the significance level at 0.05, the most significant main effects were found to be [Zn+Al], 2[CO_3^{2-}]/[Zn+Al], and addition rate, with an important interaction of [Zn+Al]*stirring rate (Table S1).

In order to retain the hierarchy, a linear regression model of the MPS, with all the significant effects and interaction (i.e., [Zn+Al], 2[CO_3^{2-}]/[Zn+Al], addition rate and [Zn+Al]*stirring rate) along with the stirring rate, was developed by fitting the data using the least square method. The model with R^2 (square of the correlation coefficient) of 0.997 and R_{adj}^2 (square of the adjusted correlation coefficient) of 0.990 is expressed as:

$$\begin{aligned} MPS = 481.3 + 5.73(C_{salt} - 35) - 439.67(n_{cs} \\ - 0.15) - 0.079(S_{sitr} \\ - 1150) - 182.37(S_{add} \\ - 0.416) + 0.011(C_{salt} - 35)(S_{stir} - 1150) \end{aligned} \quad (1)$$

where *MPS* is the mean particle size in nm, C_{salt} is [Zn+Al] in mM, n_{cs} is the molar ratio of 2[CO_3^{2-}]/[Zn+Al], S_{stir} is the stirring rate in rpm, and S_{add} is the addition rate in ml/s. Note,

R^2 reflects the proportion of the variation in MPS that can be attributed to the model parameters rather than to random error, and R^2_{adj} is the adjusted R^2; the closeness of R^2 and R_{adj}^2 and having a magnitude of 1 indicate accuracy.

The importance of significant main effects and interaction parameters, denoted in the empirical model (equation 1), is clearly reflected in the leverage plots (Figure 1) with their confidence curves (at 5% level) represented in dash lines. Here, the slope represents the degree of influence on the MPS. The exclusion of the horizontal line from the confidence region for [Zn+Al] and 2[CO_3^{2-}]/[Zn+Al], and close to inclusion of the horizontal line from the confidence region for addition rate and [Zn+Al]*stirring rate, are indicative of significance and borderline significance, respectively. The salt concentration is closely related to the MPS, and as shown in Figure 1a, lower [Zn+Al] leads to a smaller MPS. However, such [Zn+Al]-MPS relationship resulted from coprecipitation can be completely masked by an overwhelming HT, perhaps due to severe Ostwald's ripening. As illustrated by Ogawa and Kaiho,[29] the effect of salt concentration was completely reversed when an overwhelming HT at 100 °C for 24 h was used; they synthesized micrometer-sized (Mg, Al)-LDH particles which increased in size with decreased salt concentration. The influence of the intercalated anion on the MPS is also considerable (Figure 1b), and a stronger interaction between the anions and the double hydroxide layers (as Cl^- is partially substituted by CO_3^{2-}) leads to the diminution of MPS. This result is apparently contrary to the expectations since the nucleation rate is more or less the same due to identical supersaturation level, and the presence of CO_3^{2-}, exhibiting a very strong electrostatic interaction with the hydroxide layers, should have facilitated a more rapid growth leading to a larger MPS. This conundrum indicates that a more complex growth evolution than that just described by classical nucleation and growth is in effect. A detailed study on the formation mechanism of LDH NPs was carried out and revealed the intercalating anion composition-dependent growth mechanisms; details reported in Part 2.[ref] Figure 1c and 1d shows the inverse and direct relationships (although mild) of addition rate and [Zn+Al]*stirring rate with the MPS, respectively.

Figure 2 shows the 2^{4-1} design representation and chi-squared (χ^2) plots of PSD as a function of the main effects. Here, χ^2 is used as the key indicator for goodness of fit of PSD to the Gaussian distribution; test of a good fit is a low χ^2 (ideally < 3).[36] At first glance, the deviation from the ideal Gaussian PSD is distinct with [Zn+Al]. Figure 2a and 2d, for low and high [Zn+Al], clearly shows that a higher stirring rate can lead to PSD with smaller χ^2. Figure 2c and 2f, for low and high [Zn+Al], indicates that PSD of LDH NPs synthesized in the presence of a high level of 2[CO_3^{2-}]/[Zn+Al] tend to have larger χ^2 than in the absence of CO_3^{2-}. However, a closer examination reveals that even when the LDH NPs are synthesized under high 2[CO_3^{2-}]/[Zn+Al], a higher stirring rate can significantly reduce χ^2 (e.g. Run 1 and Run 3). In contrast, for low and high [Zn+Al], the addition rate does not exhibit obvious trends (figure 2b and 2e). Therefore, among the screening parameters, the main effects that markedly influence PSD are determined to be the [Zn+Al] and stirring rate; note, an optimum coprecipitation conditions to achieve an ideal PSD would be a relatively low [Zn+Al] and more importantly, a high stirring rate.

The Gaussian analysis is limited to describing only simple particle size distributions symmetric, unimodal populations. For samples with a large value of χ^2 (>3), NICOMP analysis was used.[36, 37] Here, the percentage of the largest integral of the scattering intensity of an independent distribution among all is referred to the scattering intensity-weighed percentage of primary fraction, and is used as a quantitative indicator of the closeness to a unimodal size distribution. Figure 3 further illustrates the beneficial effects of high stirring rate on PSD. In runs 4 (i.e., no CO_3^{2-}, high addition rate, and low [Zn+Al]), 1 (i.e., high CO_3^{2-}, low addition rate, and low [Zn+Al]), and 3 (i.e., high CO_3^{2-}, high addition rate, and high [Zn+Al]), a high stirring rate leads to almost monodispersed PSD. The importance of high stirring rates has also been mentioned for the synthesis of various NPs, e.g., $BaTiO_3$[38] and Fe_3O_4.[39, 40] In essence, a high stirring rate ensures rapid and complete mixing of precursors, reduces the time variation of the homogeneous nucleation and growth events, enables the formation of a single and narrow PSD, and facilitates the formation of phase-pure LDH over individual hydroxides.

3.2. Understanding hydrothermal treatment (HT) and its optimization

The coprecipitation at RT always led to severe agglomeration of amorphous (Zn, Al)-LDH NPs, which resulted in a large MPS and non-Gaussian PSD. Hence, as past literatures have demonstrated, HT in the absence of convection is necessary to form crystalline LDH NP suspensions. During HT of agglomerated amorphous LDH NPs, the formation of crystalline LDH NPs and the dispersion to form stable colloidal suspensions can perhaps be explained by phase transformation and the consequent change in surface energy mediated by the change in surface charge and hydration tendency.[41–44] The as-coprecipitated metastable amorphous LDH NPs tend to have a lower number of high-energy sites (i.e., charged sites) per unit surface area, compared to the thermodynamically stable crystalline counterpart. Consequently, hydration on a smaller number of these sites leads to a low hydration enthalpy, which makes agglomeration the principle mechanism for further lowering the energy of the amorphous phase. The t_{HT} and T_{HT}-dependent HT can transform the metastable phase to the thermodynamically stable crystalline LDH NPs through atomic rearrangement of the bulk coupled with a surface dissolution-reprecipitation process. The presence of a higher number of charged sites on crystalline NPs leads to repulsion between NPs and increased hydration. Consequently, the high hydration enthalpy lowers the energy of the system to the extent that agglomeration is unnecessary. Moreover, one must be aware that particle coarsening can also occur during HT, perhaps initially via diffusive growth mechanism.[33] As crystalline perfection increases, the energetic costs to incorporate atoms into larger NPs or detach atoms from smaller NPs can lead an interface-driven coarsening mechanism.[33] In essence, suitable HT conditions (i.e., T_{HT} and t_{HT}) are critical to improve crystallinity, form stable colloidal suspensions by electrostatic stabilization, and obtain monodispersed PSD.

Since the HT conditions for the screening experiments were not at their optima, the optimization of this step was essential. Note, a too low T_{HT} (< 50 °C) was insufficient to transform the metastable phase to the most thermodynamically stable crystalline phase (e.g., at 51 °C, it takes > 7 h to re-disperse the agglomerated amorphous NPs into crystalline forms; data shown in Part 2).[ref] A too high T_{HT} (> 90 °C) enhanced Ostwald ripening that

led to larger disparities in particle size with time, and caused compositional change in growing particles due to the difference in the reprecipitation rates of the divalent and trivalent cations. Also, agglomeration was observed,[ref] in addition to the potential activation of the condensation reactions of Zn-OH via dehydration to form additional ZnO phase in aqueous media.[34] Moreover, based on numerous previous runs, crystallization at 60–85 °C is completed within 2–6 h, but prolonged HT masks the results of initial coprecipitation due to significant coarsening. Therefore, to determine the optimum HT conditions, these samples were treated at 70 and 85 °C for 3, 5 and 8 h. The results are illustrated in Table 2.

Clearly, the monodispersed Gaussian distribution with the lowest χ^2 can be achieved by treating the sample at 85 °C for as little as 5 h. Relatively low T_{HT} (70–85 °C) only allowed a slow coarsening process (i.e., particle growth), as shown by the comparison between the samples treated at 85 °C for 5 and 8 h. Note, although the optimum HT can improve the PSD towards monodispersion, the extent of its efficacy is limited by how ideal the prior coprecipitation conditions are.

3.3. Quantitative model development using central composite design

Here a more elaborate central composite design with two central points was employed for higher resolution to construct the response surface. The selected main factors with their adjusted ranges for the model were [Zn+Al] (5–45 mM) and 2[CO_3^{2-}]/[Zn+Al] (0–0.3), along with the borderline factor of addition rate (0.243–0.589 ml/s), included here due to the projection property of the factorial design. Also, based on the results of screening, the highest permissible stirring rate of 3000 rpm of the current stirrer was chosen for all the runs. The experiments were carried out following the aforementioned procedure, followed by a HT at 85 °C for 5 h. Table S2 summarizes the coprecipitation conditions and results for the 16 runs.

Based on the data shown in Table S2, a simple model ($\alpha = 0.05$) that predicts MPS was developed, where no interaction effect was significant, and R^2 and R_{adj}^2 were 0.978 and 0.972, respectively. The model can be expressed as follows:

$$MPS = 371.71 + 4.8(C_{salt} - 20) - 291.53(n_{cs} - 0.15) - 93.24(S_{add} - 0.416) \quad (2)$$

According to the leverage plots shown in Figure 4, [Zn+Al] and 2[CO_3^{2-}]/[Al] are significant and the addition rate is at the borderline of significance, consistent with screening results.

A surface plot and two-dimensional response contours of the MPS, for a fixed addition rate (0.589 ml/s), are shown in Figure 5a and *b*, respectively. Here the MPS range (~ 200–500 nm) is readily controlled through two easily controllable processing parameters of [Zn+Al] and 2[CO_3^{2-}]/[Al].

The validity of this model was tested by selecting a few points (I to VI shown as solid circles in Figure 5b) and carrying out synthesis of Cl^--intercalated (Zn, Al)-LDH NPs under the specified conditions, followed by the comparison of the MPS predicted by the model

with the experimental results. After coprecipitation, all samples were hydrothermally treated at 85 °C for 5 h. The bright field TEM images of nearly monodispersed (Zn, Al)-LDH NPs of various particle sizes are displayed in Figure 6a. The NPs were LDH phase-pure and single crystalline. A representative X-ray diffraction pattern and electron diffraction pattern for Sample VI (with d_{003} of 7.7 Å) are depicted in Figure 6b and 6c, respectively.

Table 3 clearly shows the close correspondence of the MPS predicted by the model with the experimental TEM results, computed by averaging the largest dimension of individual LDH nanoparticles. The comparisons of sample III with IV and V with VI show that the presence of a small amount of CO_3^{2-} within the gallery spacing stabilizes the LDH NPs under hydrothermal conditions and minimizes the coarsening process. The less stable sample IV and VI were more susceptible to the Ostwald ripening,[33] and as a result, a wider range of particle size was observed.

3.4. Evaluation of the effect of [Zn]/[Al] molar ratio on the resultant particle size

The effect of the [Zn]/[Al] molar ratio on the particle size of Cl^--intercalated (Zn, Al)-LDH NPs were studied by changing the input [Zn]/[Al] ratio from 1 to 4. The coprecipitation conditions were as follows: [Zn+Al] of 5 mM, [NaOH]/[Zn+Al] of 2, 2[CO_3^{2-}]/[Al] of 0.3, stirring rate of 3000 rpm, addition rate of 0.589 ml/s and HT conditions of 85 °C for 5 h. Having collected the NPs after centrifugation, the phase purity of LDH was determined by XRD in the 2θ range of 7–70°. The actual compositions determined by ICP, for [Zn]/[Al] molar ratios of 1 to 4, were $Zn_{0.509}Al_{0.491}(OH)_2(CO_3^{2-})_{0.074}Cl_{0.344}{\cdot}xH_2O$, $Zn_{0.656}Al_{0.344}(OH)_2(CO_3^{2-})_{0.052}\ Cl_{0.241}{\cdot}xH_2O$, $Zn_{0.724}Al_{0.276}(OH)_2(CO_3^{2-})_{0.041}Cl_{0.193}{\cdot}xH_2O$ and $Zn_{0.781}\ Al_{0.219}\ (OH)_2\ (CO_3^{2-})_{0.033}Cl_{0.153}{\cdot}xH_2O$, respectively. Figure 7 illustrates the effect of [Zn]/[Al] ratio on the zeta-potential and mean hydrodynamic particle size. All the samples exhibited a monodispersed PSD except for the $Zn_{0.781}\ Al_{0.219}\ (OH)_2\ (CO_3^{2-})_{0.033}Cl_{0.153}{\cdot}xH_2O$ sample synthesized with a [Zn]/[Al] ratio of 4, and the mean hydrodynamic particle size increased with [Zn]/[Al] ratio. Similar phenomenon has been demonstrated in a study of cationic composition-morphology of (Mg, Al)-LDH system using nanoseparation technique.[45] The large particle size (~1.7 μm in diameter) of the $Zn_{0.781}\ Al_{0.219}\ (OH)_2\ (CO_3^{2-})_{0.033}Cl_{0.153}{\cdot}xH_2O$ sample can be attributed to the poor long-term stability and agglomeration due to the low zeta-potential that results from the low trivalent Al^{3+} content. Therefore, from the view point of stabilization by surface charges, the suitable range of [Zn]/[Al] ratio should be 1–3. When the M^{2+} to M^{3+} ratio is close to 1, the resulting precipitate may be disordered,[2] but such a result is highly contingent on the synthesis conditions, i.e., precursor type, coprecipitation pH, and HT regimen. For example, crystalline nanoparticles of $[Mg_{0.56}Al_{0.44}(OH)_2]^{0.44}[0.22X^-{\cdot}nH_2O]$, where $X^- = ½CO_3^{2-}$ or OH^-, have been successfully synthesized.[46]

4. Conclusions

With the aid of statistical design of experiments, the controlled synthesis of single crystalline Cl^--intercalated (Zn, Al)-LDH NPs was achieved using coprecipitation at constant pH followed by HT. Among various screening factors, a high stirring rate was identified as the critical parameter to obtain a monodispersed PSD. Here, the highest

achievable stirring rate was limited by the stirrer used, and it is envisioned that stirring rates > 3000 rpm could further reduce the width of the PSD, especially for high [Zn+Al]. A quantitative MPS model, expressed in terms of the significant factors, was developed and used to synthesize nearly monodispersed LDH NPs with MPS anywhere in the range of 200–500 nm by controlling the [Zn+Al], 2[CO_3^{2-}]/[Zn+Al], and the addition rate.

Another interesting finding was that a stronger interaction between the intercalated anion and double hydroxide layers led to a smaller particle size, i.e., when Cl^- is partially replaced by CO_3^{2-}. Such a phenomenon is apparently contradictory to classical nucleation and growth, and the details of this intercalating anion composition-dependent growth mechanisms are reported in Part 2.[ref]

Moreover, the ideal range of [Zn]/[Al] molar ratio for obtaining (Zn, Al)-LDH NPs was determined to be between 1 and 3, with ratios approaching 4 leading to a dramatic increase in particle size. From a practical point of view, the current methodology can be used to optimize the synthesis parameters of other biocompatible LDH NPs.

Supplementary Material

Refer to Web version on PubMed Central for supplementary material.

Acknowledgments

SKD acknowledges financial support from the National Cancer Institute, National Institutes of Health (1R21CA133618), National Science Foundation (CBET-0829128), and ASU Foundation's Women & Philanthropy (WZ91010). The authors gratefully acknowledge the use of facilities within the LeRoy Eyring Center for Solid State Science at Arizona State University, and are grateful to Dr. Thomas Groy, Dr. Robert Wang, and Dr. Karl Weiss of ASU for assistance with XRD, DLS, and TEM.

References

1. Allmann R. DOUBLE LAYER STRUCTURES WITH LAYER IONS (ME(II)(1-X)ME(III)(X)(OH)2)(X+) OF BRUCITE TYPE. Chimia. 1970; 24:99.
2. Cavani F, Trifiro F, Vaccari A. HYDROTALCITE-TYPE ANIONIC CLAYS: PREPARATION, PROPERTIES AND APPLICATIONS. Catalysis Today. 1991; 11:173–301.
3. Newman SP, Jones W. Synthesis characterization and applications of layered double hydroxides containing organic guests. New Journal of Chemistry. 1998; 22:105–115.
4. Vaccari A. Clays and catalysis: a promising future. Applied Clay Science. 1999; 14:161–198.
5. Sels BF, De Vos DE, Jacobs PA. Hydrotalcite-like anionic clays in catalytic organic reactions. Catalysis Reviews-Science and Engineering. 2001; 43:443–488.
6. Sels B, De Vos D, Buntinx M, Pierard F, Kirsch-De Mesmaeker A, Jacobs P. Layered double hydroxides exchanged with tungstate as biomimetic catalysts for mild oxidative bromination. Nature. 1999; 400:855–857.
7. Cantrell DG, Gillie LJ, Lee AF, Wilson K. Structure-reactivity correlations in MgAl hydrotalcite catalysts for biodiesel synthesis. Applied Catalysis a-General. 2005; 287:183–190.
8. Li DA, Zhang YT, Yu M, Guo J, Chaudhary D, Wang CC. Cancer therapy and fluorescence imaging using the active release of doxorubicin from MSPs/Ni-LDH folate targeting nanoparticles. Biomaterials. 2013; 34:7913–7922. [PubMed: 23886730]
9. Wang LJ, Xing HY, Zhang SJ, Ren QG, Pan LM, Zhang K, Bu WB, Zheng XP, Zhou LP, Peng WJ, Hua YQ, Shi JL. A Gd-doped Mg-Al-LDH/Au nanocomposite for CT/MR bimodal imagings and simultaneous drug delivery. Biomaterials. 2013; 34:3390–3401. [PubMed: 23380358]

10. Del Hoyo C. Layered double hydroxides and human health: An overview. Applied Clay Science. 2007; 36:103–121.
11. Panda HS, Bahadur D. Study of the preparation, properties and kinetics of anion release in drug intercalated magnetic nanohybrids. Materials Research Bulletin. 2012; 47:571–579.
12. Huang HC, Barua S, Sharma G, Dey SK, Rege K. Inorganic nanoparticles for cancer imaging and therapy. Journal of Controlled Release. 2011; 155:344–357. [PubMed: 21723891]
13. Choy JH, Kwak SY, Jeong YJ, Park JS. Inorganic layered double hydroxides as nonviral vectors. Angewandte Chemie-International Edition. 2000; 39:4042–4045.
14. Kriven WM, Kwak SY, Wallig MA, Choy JH. Bio-resorbable nanoceramics for gene and drug delivery. Mrs Bulletin. 2004; 29:33–37.
15. Wei PR, Cheng SH, Liao WN, Kao KC, Weng CF, Lee CH. Synthesis of chitosan-coated near-infrared layered double hydroxide nanoparticles for in vivo optical imaging. Journal of Materials Chemistry. 2012; 22:5503–5513.
16. Musumeci AW, Schiller TL, Xu ZP, Minchin RF, Martin DJ, Smith SV. Synthesis and Characterization of Dual Radiolabeled Layered Double Hydroxide Nanoparticles for Use in In Vitro and In Vivo Nanotoxicology Studies. Journal of Physical Chemistry C. 2010; 114:734–740.
17. Li A, Qin LL, Wang WR, Zhu RR, Yu YC, Liu H, Wang SL. The use of layered double hydroxides as DNA vaccine delivery vector for enhancement of anti-melanoma immune response. Biomaterials. 2011; 32:469–477. [PubMed: 20934217]
18. Qin LL, Xue M, Wang WR, Zhu RR, Wang SL, Sun J, Zhang R, Sun XY. The in vitro and in vivo anti-tumor effect of layered double hydroxides nanoparticles as delivery for podophyllotoxin. International Journal of Pharmaceutics. 2010; 388:223–230. [PubMed: 20045452]
19. Silion M, Hritcu D, Jaba IM, Tamba B, Ionescu D, Mungiu OC, Popa IM. In vitro and in vivo behavior of ketoprofen intercalated into layered double hydroxides. Journal of Materials Science-Materials in Medicine. 2010; 21:3009–3018. [PubMed: 20820886]
20. Braterman, PS.; Xu, ZP.; Yarberry, F. Handbook of Layered Materials. Auerbach, SM.; Carrado, KA.; Dutta, PK., editors. Marcel Dekker; New York: 2004.
21. Boclair JW, Braterman PS. Layered double hydroxide stability. 1. Relative stabilities of layered double hydroxides and their simple counterparts. Chemistry of Materials. 1999; 11:298–302. [PubMed: 11542280]
22. Boclair JW, Braterman PS, Jiang JP, Lou SW, Yarberry F. Layered double hydroxide stability. 2. Formation of Cr(III)-containing layered double hydroxides directly from solution. Chemistry of Materials. 1999; 11:303–307. [PubMed: 11542281]
23. Dey SK, Sistiabudi R. Ceramic nanovector based on layered double hydroxide: attributes, physiologically relevant compositions and surface activation. Materials Research Innovations. 2007; 11:108–117.
24. Porter, DA.; Easterling, KE. Phase Transformation in Metals and Alloys. Chapman & Hall; UK: 1996. Phase Transformation in Metals and Alloys.
25. Matijevic E. UNIFORM INORGANIC COLLOID DISPERSIONS - ACHIEVEMENTS AND CHALLENGES. Langmuir. 1994; 10:8–16.
26. Costantino U, Marmottini F, Nocchetti M, Vivani R. New synthetic routes to hydrotalcite-like compounds - Characterisation and properties of the obtained materials. European Journal of Inorganic Chemistry. 1998:1439–1446.
27. Zhao Y, Li F, Zhang R, Evans DG, Duan X. Preparation of layered double-hydroxide nanomaterials with a uniform crystallite size using a new method involving separate nucleation and aging steps. Chemistry of Materials. 2002; 14:4286–4291.
28. Xu ZP, Stevenson GS, Lu CQ, Lu GQM, Bartlett PF, Gray PP. Stable suspension of layered double hydroxide nanoparticles in aqueous solution. Journal of the American Chemical Society. 2006; 128:36–37. [PubMed: 16390109]
29. Ogawa M, Kaiho H. Homogeneous precipitation of uniform hydrotalcite particles. Langmuir. 2002; 18:4240–4242.
30. Wang Q, Tang SVY, Lester E, O'Hare D. Synthesis of ultrafine layered double hydroxide (LDHs) nanoplates using a continuous-flow hydrothermal reactor. Nanoscale. 2013; 5:114–117. [PubMed: 23128781]

31. Bellezza F, Cipiciani A, Costantino U, Nocchetti M, Posati T. Hydrotalcite-Like Nanocrystals from Water-in-Oil Microemulsions. European Journal of Inorganic Chemistry. 2009:2603–2611.
32. Chang Z, Evans DG, Duan X, Vial C, Ghanbaja J, Prevot V, de Roy M, Forano C. Synthesis of Zn-Al-CO3 layered double hydroxides by a coprecipitation method under steady-state conditions. Journal of Solid State Chemistry. 2005; 178:2766–2777.
33. Ratke, L.; Voorhees, PW. Springer. Growth and Coarsening-Ostwald Ripenning in Material Processing. 2002.
34. Vayssieres L. Growth of arrayed nanorods and nanowires of ZnO from aqueous solutions. Advanced Materials. 2003; 15:464–466.
35. JMP 10 Design of Experiments Guide, 2012
36. NICOMP 380 DLS User Manual, Particle Sizing Systems, Inc., 2006.
37. TN 302 Nicomp DLS Intensity, Volume, and Number-Weighted Gaussian Distributions.
38. Ould-Ely T, Luger M, Kaplan-Reinig L, Niesz K, Doherty M, Morse DE. Large-scale engineered synthesis of BaTiO3 nanoparticles using low-temperature bioinspired principles. Nature Protocols. 2011; 6:97–104. [PubMed: 21212785]
39. Sun J, Zhou SB, Hou P, Yang Y, Weng J, Li XH, Li MY. Synthesis and characterization of biocompatible Fe3O4 nanoparticles. Journal of Biomedical Materials Research Part A. 2007; 80A: 333–341. [PubMed: 17001648]
40. Karaagac O, Kockar H. Effect of Synthesis Parameters on the Properties of Superparamagnetic Iron Oxide Nanoparticles. Journal of Superconductivity and Novel Magnetism. 2012; 25:2777–2781.
41. Navrotsky A. Energetics of nanoparticle oxides: interplay between surface energy and polymorphism. Geochemical Transactions. 2003; 4:34–37.
42. Navrotsky A. Energetic clues to pathways to biomineralization: Precursors, clusters, and nanoparticles. Proc Natl Acad Sci USA. 2004; 101:12096–12101. [PubMed: 15297621]
43. Navrotsky A, Ma C, Lilova K, Birkner N. Nanophase transition metal oxides show large thermodynamically driven shifts in oxidation-reduction equilibria. Science. 2010; 330:199–201. [PubMed: 20929770]
44. Navrotsky A. Nanoscale effects on thermodynamics and phase equilibria in oxide systems. ChemPhysChem. 2011; 12:2207–2215. [PubMed: 21744459]
45. Chang Z, Wu C, Song S, Kuang Y, Lei X, Wang L, Sun X. Synthesis Mechanism Study of Layered Double Hydroxides Based on Nanoseparation. Inorganic Chemistry. 2013; 52:8694–8698. [PubMed: 23879682]
46. Pausch I, Lohse HH, Schurmann K, Allmann R. SYNTHESES OF DISORDERED AND A1-RICH HYDROTALCITE-LIKE COMPOUNDS. Clays and Clay Minerals. 1986; 34:507–510.

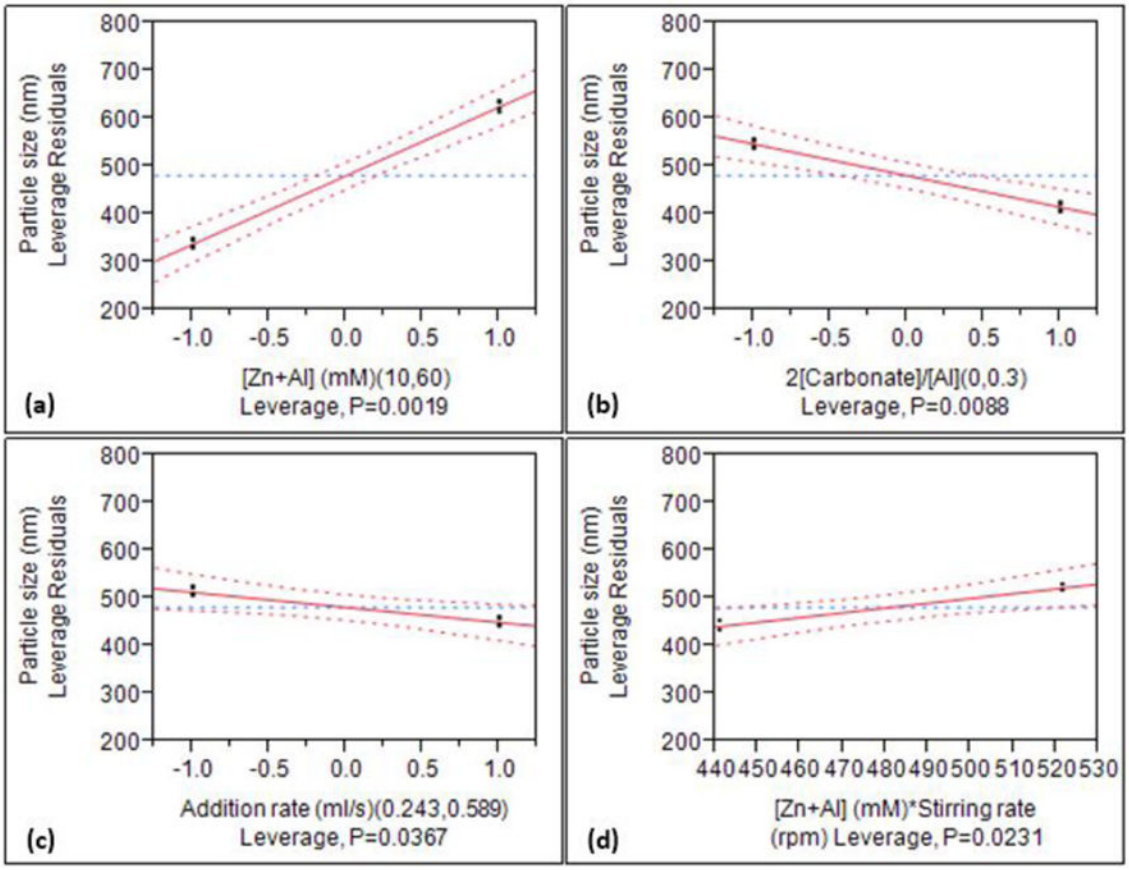

Figure 1.
Preliminary identification of the critical factors, and their trends and leverages on the MPS

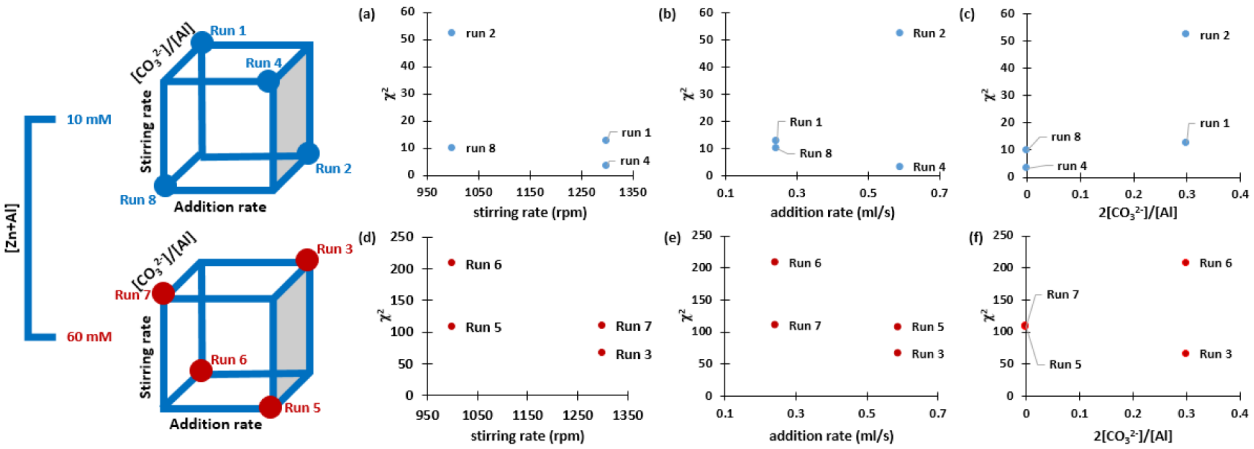

Figure 2.

Scheme of the 2^{4-1} design with resolution IV, and the graphical representations of χ^2 as functions of [Zn+Al], addition rate, stirring rate, and $2[CO_3^{2-}]/[Zn+Al]$

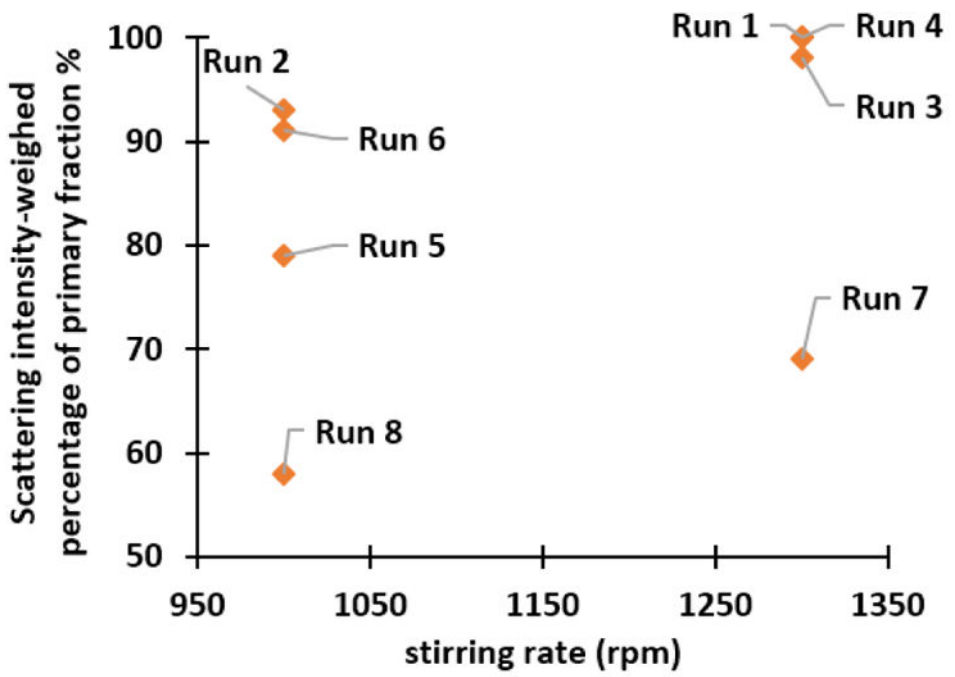

Figure 3.
Scattering intensity-weighed percentage of the primary fraction as a function of the stirring rate

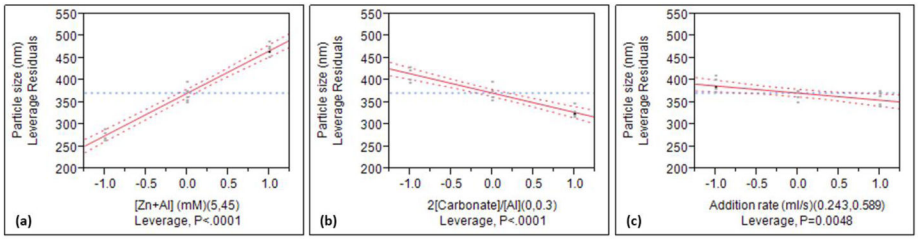

Figure 4.
Leverage residuals of the significant factors

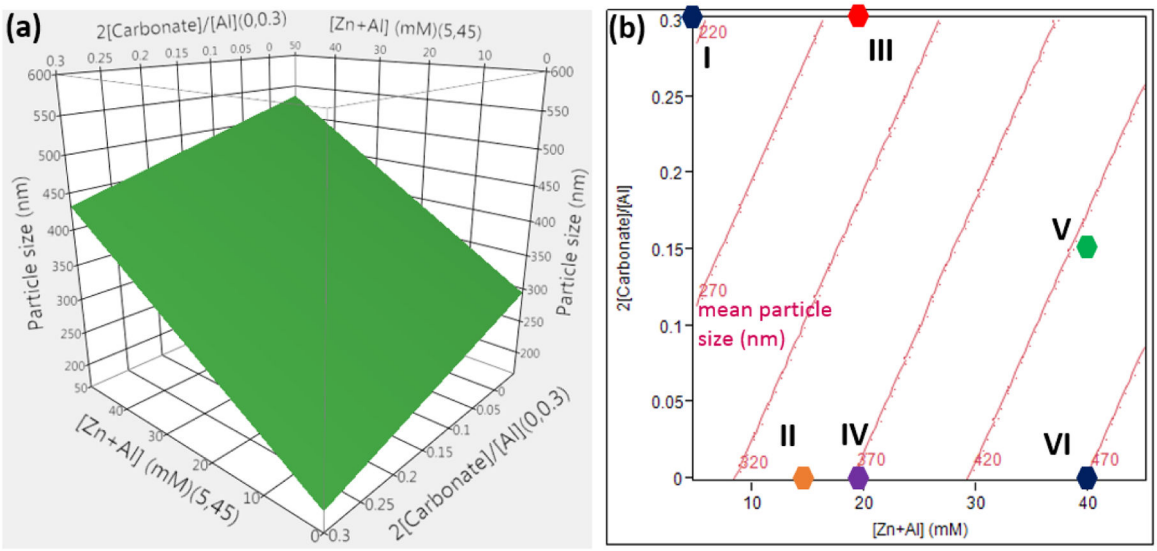

Figure 5.

Surface plot and response contours of the MPS as a function of [Zn+Al] (mM) and $2[CO_3^{2-}]/[Al]$, generated at a fixed addition rate of 0.589 ml/s and stirring rate of 3000 rpm, are shown in (a) and (b), respectively.

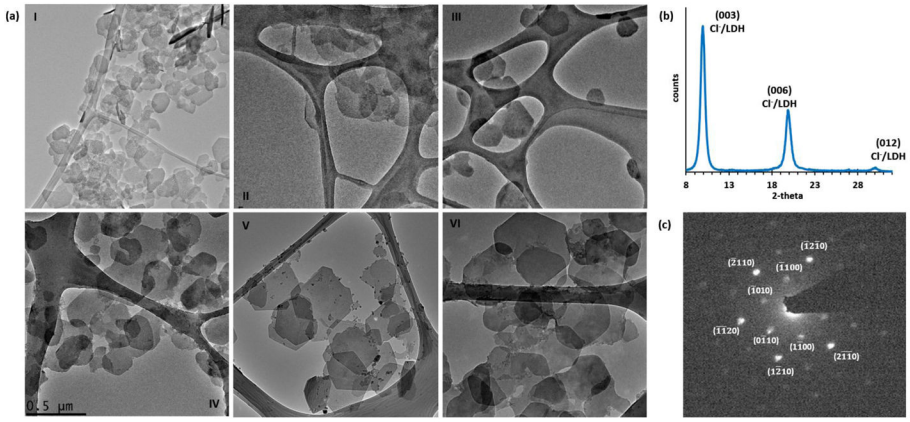

Figure 6.

(a) TEM micrographs of (Zn, Al)-LDH NPs of different particle sizes corresponding to Sample I-Sample VI, (b) XRD pattern of Sample VI, and (c) its corresponding diffraction pattern with [0001] zone axis

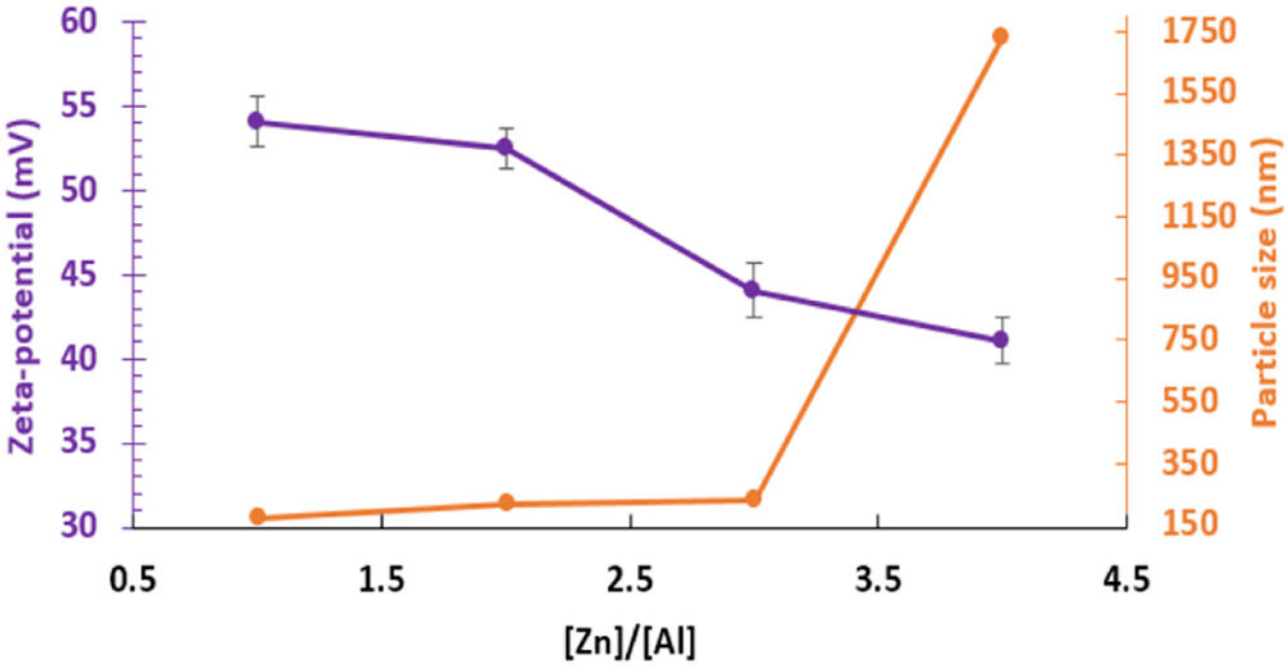

Figure 7.
Zeta-potential and particle size determined by DLS as a function of [Zn]/[Al] ratio.

Table 1

2^{4-1} design for screening: coprecipitation conditions (with HT at 70 °C for 7 h) and results

Run	Pattern	[Zn+Al] (mM)	Molar ratio 2[CO_3^{2-}]/[Al]	Stirring rate (rpm)	Addition rate (ml/s)	Mean particle size* (nm)	Major size distribution %	Chi squared χ^2
1	−++ −	10	0.3	1300	0.243	241	100	12.48
2	−+−+	10	0.3	1000	0.589	286	93	52.3
3	++++	60	0.3	1300	0.589	562	98	65.7
4	−−++	10	0	1300	0.589	331	100	3.18
5	+−−+	60	0	1000	0.589	620	79	107.71
6	++−−	60	0.3	1000	0.243	572.4	91	207.72
7	+−+−	60	0	1300	0.243	744	69	109.5
8	−−−−	10	0	1000	0.243	494	58	9.89

*Gaussian MPS is used if $\chi^2 \leq 3$; MPS fitted by NICOMP method is used when $\chi^2 > 3$. [36]

Table 2

Results of HT applied to the sample synthesized using the optimum coprecipitation condition (i.e., stirring rate of 2250 rpm, [Zn+Al] of 20 mM, 2[CO_3^{2-}]/[Al] of 0.3, and addition rate of 0.416 ml/s)

	3 h	**5 h**	**8 h**
70 °C	χ^2 =35.5 NICOMP: 50 nm (15.6%) 322.5 nm (84.4%)	χ^2 = 2.34 Gaussian: 327.4 nm	χ^2 = 1.68 Gaussian: 309 nm
85 °C	χ^2 =33.31 NICOMP: 114.1 nm (8.06%) 341.6 nm (91.64%)	χ^2 = 0.90 Gaussian: 303.4 nm	χ^2 = 1.32 Gaussian: 323 nm

Table 3

Comparison of the predicted MPS and particle size determined by TEM bright field micrograph

Sample	I	II	III	IV	V	VI
Predicted MPS (nm)	216	351	288	375	428	471
TEM determined MPS (nm)	189	344	252	354	398	466